AIMS Mathematics, 10(11): 27696–27717.
DOI: 10.3934/math.20251218
Received: 01 September 2025
Revised: 11 November 2025
Accepted: 17 November 2025
Published: 27 November 2025

https://www.aimspress.com/journal/Math

Research article

Mathematical modeling of alcohol-induced effects on bone remodeling dynamics

Inthira Chaiya[1,*], Teeraporn Kaewkrathok[1], Apasara Ploykanha[1], Din Prathumwan[2] and Kamonchat Trachoo[1]

[1] Department of Mathematics, Faculty of Science, Mahasarakham University, Mahasarakham, 44150, Thailand

[2] Department of Mathematics, Faculty of Science, Khon Kaen University, Khon Kean, 40002, Thailand

* **Correspondence:** Email: inthira.c@msu.ac.th; Tel: +6643754244; Fax: +6643754244.

Abstract: This study develops a mathematical model to investigate the impact of alcohol consumption on bone remodeling dynamics, thereby focusing on osteoclast, osteoblast, and bone mass interactions. Extending Komarova's framework, the model incorporates alcohol-dependent regulatory factors which influence cell proliferation and apoptosis. Analytical methods are used to determine the steady states and assess the local stability via the Jacobian matrix, while numerical simulations in MATLAB illustrate the system behavior under varying alcohol levels. The results show that moderate alcohol intake supports stable and periodic remodeling, whereas excessive or insufficient consumption disrupts the equilibrium, which leads to bone loss. These findings provide quantitative insights into alcohol-induced bone disorders and highlight the importance of maintaining moderate alcohol consumption for skeletal health.

Keywords: mathematical model; bone remodeling; alcohol; stability
Mathematics Subject Classification: 92-10, 92C37, 92C50, 37N25

1. Introduction

Bones are essential tissues that serve as the structural framework of the human body and act as reservoirs for various critical minerals, thus contributing to the body's mineral balance. The maintenance of bone strength heavily relies on the process of bone remodeling, which is a dynamic and continuous process that occurs throughout human life. Bone remodeling involves the coordinated actions of several bone cells. Osteocytes, which act as mechanosensors, detect mechanical stress and damage, thus initiating the remodeling process. Osteoclasts break down old or damaged bone tissue,

while osteoblasts generate new bone tissue to replace the resorbed bone. These two cell types work together at specific sites known as basic multicellular units (BMUs).

The bone remodeling process can be divided into four main phases. The first phase involves the activation of BMUs, where cells that give rise to osteoblasts separate, thus exposing the bone surface. The release of the receptor activator of nuclear factor kappa-B ligand (RANKL) attracts osteoclast precursor cells to this exposed bone surface. In the second phase, RANKL, produced by osteoblasts, binds to RANK receptors on osteoclast precursor cells, thus stimulating their differentiation into mature osteoclasts that resorb bone tissue. At the same time, osteoblast lineage cells produce osteoprotegerin (OPG), a protein that inhibits RANKL–RANK binding, thereby regulating osteoclast development and function. The third phase prepares the bone surface for the formation of new bone and may involve signals that stimulate osteoblast differentiation. Finally, during bone formation, mesenchymal stem cells differentiate into osteoblasts, which synthesize and deposit proteins that later mineralize with calcium and phosphorus. Therefore, effective communication between osteoclasts and osteoblasts is essential to maintain skeletal balance, and any disruption can lead to bone diseases such as osteoporosis [1].

Bone strength is commonly assessed by the bone mineral density (BMD), which represents the mineral concentration that determines bone rigidity [2]. For women, normal bone mass ranges from 1.95 to 2.90 kg, depending on body weight, and from 2.65 to 3.69 kg for men [3]. The World Health Organization (WHO) classifies BMD using the T-score, which compares an individual's BMD with that of a healthy young adult: a T-score between -1 and 1 indicates normal bone health, between -2.5 and -1 indicates osteopenia, and below -2.5 indicates osteoporosis [4].

Chronic alcohol consumption has been shown to impair bone health by inducing osteocyte apoptosis and increasing the secretion of sclerostin, which inhibits Wnt signaling, thereby reducing osteoblast proliferation and bone formation. Additionally, alcohol stimulates the production of IL-6, which promotes RANKL activation and inhibits OPG production, thus leading to enhanced osteoclastogenesis and bone resorption [5].

Experimental evidence supports these effects. Individuals who abstain from alcohol exhibit the highest bone mass ($18.8 \pm 1.7\%$), while moderate (80–130 g/day) and heavy drinkers (more than 130 g/day) show significantly lower averages [6]. Similarly, alcohol consumption above 57.2 g per week correlates with a reduced bone mass in older women [7], whereas moderate drinking—up to 8 g/day for women and 16 g/day for men—has been associated with a higher BMD [8]. Hence, maintaining moderate alcohol intake appears beneficial, while excessive consumption accelerates bone loss [5].

Despite significant advances in understanding the biochemical pathways which underlie alcohol-induced bone loss, the quantitative characterization of how varying alcohol levels dynamically alter bone remodeling remains limited. Existing research is largely experimental or descriptive, lacking the predictive capability to capture nonlinear feedback between osteoclasts, osteoblasts, and bone mass over time. This motivates the development of mathematical models that integrate biological mechanisms with alcohol exposure dynamics to predict long-term effects on bone health.

Mathematical modeling provides a powerful approach to explore regulatory mechanisms in bone remodeling and predicting pathological changes. Komarova [9] first formulated a system of ordinary differential equations (ODEs) that described osteoclast–osteoblast interactions and bone mass regulation. Jerez and Chen [10] later investigated its stability, while Lio et al. [11] incorporated

osteocyte feedback and cellular degradation to better represent osteoporotic bone loss. Javed et al. [12] extended these models to include therapeutic interventions, thus demonstrating their clinical relevance.

Recent developments have expanded these frameworks to include structural and memory effects. For instance, Trachoo et al. [13] introduced porosity-dependent dynamics in an improved ODE model, while Trachoo et al. [14] proposed a fractional-order bone remodeling model using the Atangana–Baleanu Caputo derivative to incorporate memory effects. Bahrami et al. [15] provided a comprehensive review that emphasized the need for biologically updated mathematical models.

Beyond bone remodeling, related mathematical approaches have recently been advanced in computational biology. A new mixed fractional derivative with applications in computational biology offers flexible kernel formulations for systems with long-term memory [16], and a new class of generalized fractal and fractal–fractional derivatives with non-singular kernels enables the modeling of processes with fractal space–time scaling [17]. Additionally, the stability and control analysis of delayed social epidemic models [18] provides theoretical tools for handling general contact rates, delays, and optimal control—concepts that are also relevant to delayed feedback in bone cell signaling. Collectively, these advances point to potential future directions to extend the present model toward fractional-order and delay-inclusive frameworks.

Recent works on fractional-order delayed and kinetic systems further illustrate progress in a nonlinear dynamics analysis. For example, Li et al. [19] explored the dynamics of a fractional-order delayed zooplankton–phytoplankton system, while Xu et al. [20] investigated fractional kinetic models with Ulam–Hyers stability. These studies highlight analytical techniques applicable to complex biological systems, thus offering valuable perspectives for enriching future bone remodeling models.

Complementary computational methods have also improved the model's tractability. Nave [21] proposed a modified semi-analytical method for nonlinear ODEs that enhanced the computational accuracy, potentially benefiting large-scale or parameter-sensitive bone remodeling simulations. Experimental studies also support these findings, thereby showing that binge alcohol exposure alters gene expression in osteoblast and osteoclast pathways [22], thus reinforcing the biological foundation of mathematical investigations.

While these studies collectively advance the theoretical and computational understanding, the present work is distinct in incorporating alcohol consumption as a direct regulatory factor in osteoblast–osteoclast interactions within a Komarova-type framework. By explicitly linking alcohol exposure to cell population dynamics and bone mass regulation, our model connects lifestyle behavior with quantitative bone remodeling outcomes.

Therefore, the main objective of this study is to bridge the gap between biological observations and predictive modeling by quantifying the nonlinear effects of alcohol consumption on bone remodeling. This work aims to establish a mathematical foundation to understand how different drinking patterns influence bone mass regulation and to provide insights for prevention and clinical management of alcohol-related bone disorders.

In this study, we extend Komarova's model to examine how alcohol consumption influences bone remodeling, thereby focusing on osteoclast and osteoblast population dynamics and bone mass changes over time.

2. Mathematical model

In this study, we developed a mathematical model to characterize the dynamics of bone remodeling by incorporating the populations of osteoclasts (C), osteoblasts (B), and bone density (z). This model is used to analyze the impact of alcohol consumption on the bone remodeling process, as illustrated in Figure 1.

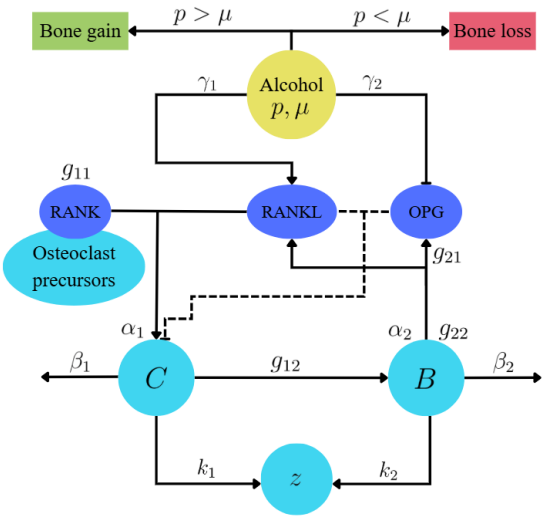

Figure 1. A diagram showing the impact of alcohol on the bone remodeling process.

The dynamics of osteoclasts, osteoblasts, and bone density are governed by the following:

$$\frac{dC}{dt} = \alpha_1 C^{g_{11}} B^{g_{21}} - \beta_1 C - \gamma_1 (p - \mu) C, \tag{2.1}$$

$$\frac{dB}{dt} = \alpha_2 C^{g_{12}} B^{g_{22}} - \beta_2 B + \gamma_2 (p - \mu) B, \tag{2.2}$$

$$\frac{dz}{dt} = -k_1 \max(C - \bar{C}, 0) + k_2 \max(B - \bar{B}, 0), \tag{2.3}$$

respectively. All parameters are positive constants, except for $g_{ij} \in \mathbb{R}$, and are defined as follows:

C	represents the number of osteoclasts,
B	represents the number of osteoblasts,
z	represents bone density,
α_1, α_2	represent the proliferation rates of osteoclasts and osteoblasts, respectively,
β_1, β_2	represent the apoptosis rates of osteoclasts and osteoblasts, respectively,
g_{ij}	represents the effect of autocrine or paracrine factors produced by osteoclasts or osteoblasts,

γ_1, γ_2	represent the increased rates of osteoclast and osteoblast production due to alcohol consumption, respectively,
p	represents the optimal alcohol consumption level,
μ	represents the amount of alcohol consumed,
k_1, k_2	represent the rates of bone resorption and bone formation, respectively,
$\bar{C}, \bar{B}$	represent the number of osteoclasts and osteoblasts at equilibrium, respectively.

Compared with existing models such as Komarova et al. [9], which described normal bone remodeling through cell-to-cell interactions, the present system (2.1)–(2.3) explicitly introduces alcohol-dependent feedback terms (γ_1, γ_2) to capture the physiological influence of alcohol on osteoclast and osteoblast activity. This extension enables a direct quantitative analysis of how varying alcohol consumption levels—from abstinence to excessive intake–affect the bone mass dynamics, thus enhancing both biological realism and interpretability.

Moreover, the effects of key cytokines (e.g., IL-6, RANKL, OPG) are implicitly incorporated through parameters g_{ij}, α_i, β_i, and γ_i. This approach maintains biological relevance while keeping the model analytically tractable. The parameter values are derived from experimental and clinical evidence [5, 6, 9].

Equation (2.1) describes the rate of change in the number of osteoclast cells, which increases due to the autocrine effect of osteoclast-secreted factors (g_{11}) and the paracrine effect of osteoblast-secreted factors (g_{21}). Consequently, the osteoclast population grows at a proliferation rate of α_1 and decreases at an apoptosis rate of β_1. Furthermore, excessive alcohol consumption $p < \mu$ leads to an additional increase in the osteoclast population at a rate of γ_1. Here, g_{11} represents the self-regulatory stimulation among osteoclasts (autocrine signaling) that enhances the bone resorption activity, whereas g_{21} denotes the influence of osteoblast-derived signaling molecules that can indirectly promote osteoclast differentiation and activation.

Equation (2.2) describes the rate of change in the number of osteoblast cells, which increases due to the paracrine effect of osteoclast-secreted factors (g_{12}) and the autocrine effect of osteoblast-secreted factors (g_{22}). Thus, the osteoblast population grows at a proliferation rate of α_2 and decreases at an apoptosis rate of β_2. Furthermore, excessive alcohol consumption $p < \mu$ leads to a reduction in the osteoblast population at a rate of γ_2. In this context, g_{12} represents the stimulatory effect of osteoclasts on osteoblasts during the bone formation phase, while g_{22} reflects the self-regulatory signaling among osteoblasts that promotes their differentiation and function. The differences among g_{11}, g_{12}, g_{21}, and g_{22} illustrate the bidirectional but asymmetric coupling between osteoclasts and osteoblasts that governs the bone remodeling dynamics.

Equation (2.3) describes the rate of change in bone mass, which decreases due to bone resorption by osteoclast cells that exceed the equilibrium point $\bar{C}$ at a resorption rate of k_1. Conversely, the bone mass increases due to bone formation by osteoblast cells that exceed the equilibrium point $\bar{B}$ at a formation rate of k_2.

3. Model analysis

In this section, we will analyze the stability of the system of Eqs (2.1) and (2.2) by isolating Eq (2.3) from the system.

3.1. Steady-state

The steady-state points are obtained by setting the time derivatives to zero as follows:

$$\frac{dC}{dt} = 0, \quad \frac{dB}{dt} = 0.$$

From the system (2.1) and (2.2), we have the following:

$$\alpha_1 C^{g_{11}} B^{g_{21}} - \beta_1 C - \gamma_1(p-\mu)C = 0, \tag{3.1}$$

$$\alpha_2 C^{g_{12}} B^{g_{22}} - \beta_2 B + \gamma_2(p-\mu)B = 0. \tag{3.2}$$

Factorizing C in (3.1) and B in (3.2) gives the following:

$$C\left(\alpha_1 C^{g_{11}-1} B^{g_{21}} - \beta_1 - \gamma_1(p-\mu)\right) = 0, \tag{3.3}$$

$$B\left(\alpha_2 C^{g_{12}} B^{g_{22}-1} - \beta_2 + \gamma_2(p-\mu)\right) = 0. \tag{3.4}$$

This leads to the following possibilities for each equation:

1. $C = 0$ or $\alpha_1 C^{g_{11}-1} B^{g_{21}} - \beta_1 - \gamma_1(p-\mu) = 0$,
2. $B = 0$ or $\alpha_2 C^{g_{12}} B^{g_{22}-1} - \beta_2 + \gamma_2(p-\mu) = 0$.

Combining these cases gives the trivial steady state

$$(C^0, B^0) = (0,0), \quad \text{if } \beta_2 - \gamma_2(p-\mu) \neq 0,$$

and the non-trivial steady state (C^*, B^*), which is obtained by solving the following algebraic system:

$$\alpha_1 C^{g_{11}-1} B^{g_{21}} - \beta_1 - \gamma_1(p-\mu) = 0,$$
$$\alpha_2 C^{g_{12}} B^{g_{22}-1} - \beta_2 + \gamma_2(p-\mu) = 0.$$

Solving this system yields the following:

$$(C^*, B^*) = \left(\left(\frac{\beta_1 + \gamma_1(p-\mu)}{\alpha_1}\right)^{\frac{1-g_{22}}{\delta}} \left(\frac{\beta_2 - \gamma_2(p-\mu)}{\alpha_2}\right)^{\frac{g_{21}}{\delta}}, \left(\frac{\beta_1 + \gamma_1(p-\mu)}{\alpha_1}\right)^{\frac{g_{12}}{\delta}} \left(\frac{\beta_2 - \gamma_2(p-\mu)}{\alpha_2}\right)^{\frac{1-g_{11}}{\delta}}\right), \tag{3.5}$$

where

$$\delta = g_{12}g_{21} - (1-g_{11})(1-g_{22}). \tag{3.6}$$

The non-trivial steady state exists under the following conditions:

$$\left(\frac{\beta_1 + \gamma_1(p-\mu)}{\alpha_1}\right)^{\frac{1-g_{22}}{\delta}} \left(\frac{\beta_2 - \gamma_2(p-\mu)}{\alpha_2}\right)^{\frac{g_{21}}{\delta}} > 0, \tag{3.7}$$

$$\left(\frac{\beta_1 + \gamma_1(p-\mu)}{\alpha_1}\right)^{\frac{g_{12}}{\delta}} \left(\frac{\beta_2 - \gamma_2(p-\mu)}{\alpha_2}\right)^{\frac{1-g_{11}}{\delta}} > 0. \tag{3.8}$$

Remark. The non-trivial steady state represents a biologically meaningful equilibrium where both cell populations coexist.

3.2. Stability at the steady-state

Considering the Jacobian matrix of system (2.1) and (2.2), we obtain the following:

$$J(C,B) = \begin{pmatrix} a_{11} & a_{12} \\ a_{21} & a_{22} \end{pmatrix}, \tag{3.9}$$

where

$$a_{11} = \alpha_1 g_{11} C^{g_{11}-1} B^{g_{21}} - \beta_1 - \gamma_1(p-\mu), \tag{3.10}$$
$$a_{12} = \alpha_1 g_{21} C^{g_{11}} B^{g_{21}-1}, \tag{3.11}$$
$$a_{21} = \alpha_2 g_{12} C^{g_{12}-1} B^{g_{22}}, \tag{3.12}$$
$$a_{22} = \alpha_2 g_{22} C^{g_{12}} B^{g_{22}-1} - \beta_2 + \gamma_2(p-\mu). \tag{3.13}$$

Theorem 3.1. *The steady-state* (C^0, B^0) *is locally asymptotically stable if*

$$-\beta_1 - \gamma_1(p-\mu) < 0 \quad \textit{and} \quad -\beta_2 + \gamma_2(p-\mu) < 0,$$

and unstable in all other cases.

Proof. To analyze the local stability of the steady state $(C^0, B^0) = (0,0)$, we compute the Jacobian matrix of the system at the following point:

$$J(C^0, B^0) = \begin{pmatrix} -\beta_1 - \gamma_1(p-\mu) & 0 \\ 0 & -\beta_2 + \gamma_2(p-\mu) \end{pmatrix}. \tag{3.14}$$

The eigenvalues of a diagonal matrix are simply the following diagonal entries:

$$\lambda_1 = -\beta_1 - \gamma_1(p-\mu), \quad \lambda_2 = -\beta_2 + \gamma_2(p-\mu).$$

A steady state is locally asymptotically stable if all eigenvalues of the Jacobian have negative real parts. Hence, the conditions for stability are as follows:

$$\lambda_1 < 0 \implies -\beta_1 - \gamma_1(p-\mu) < 0, \quad \lambda_2 < 0 \implies -\beta_2 + \gamma_2(p-\mu) < 0.$$

If either inequality fails, then at least one eigenvalue is positive, and the steady state is unstable. This completes the proof. □

Theorem 3.2. *Let* (C^*, B^*) *be the non-trivial steady state of system* (2.1) *and* (2.2). *The stability of* (C^*, B^*) *is determined by the following Jacobian matrix:*

$$J(C^*, B^*) = \begin{pmatrix} [\beta_1 + \gamma_1(p-\mu)](g_{11}-1) & g_{21}[\beta_1 + \gamma_1(p-\mu)]\dfrac{C^*}{B^*} \\ g_{12}[\beta_2 - \gamma_2(p-\mu)]\dfrac{B^*}{C^*} & [\beta_2 - \gamma_2(p-\mu)](g_{22}-1) \end{pmatrix}, \tag{3.15}$$

with the following trace and determinant:

$$\operatorname{tr}(J(C^*, B^*)) = [\beta_1 + \gamma_1(p-\mu)](g_{11}-1) + [\beta_2 - \gamma_2(p-\mu)](g_{22}-1), \tag{3.16}$$
$$\det(J(C^*, B^*)) = [\beta_1 + \gamma_1(p-\mu)][\beta_2 - \gamma_2(p-\mu)]((g_{11}-1)(g_{22}-1) - g_{12}g_{21}). \tag{3.17}$$

Consequently, the stability of (C^*, B^*) *is classified based on the sign of the trace and determinant as follows:*

1. $\det(J(C^*, B^*)) < 0$*: Saddle point (unstable).*
2. $\det(J(C^*, B^*)) > 0$, $\mathrm{tr}(J(C^*, B^*)) < 0$*: Stable node or stable spiral.*
3. $\det(J(C^*, B^*)) > 0$, $\mathrm{tr}(J(C^*, B^*)) > 0$*: Unstable node or unstable spiral.*
4. $\mathrm{tr}(J(C^*, B^*)) = 0$, $\det(J(C^*, B^*)) > 0$*: Neutral center.*

Proof. The eigenvalues of $J(C^*, B^*)$ satisfy the following:

$$\lambda_{1,2} = \frac{\mathrm{tr}(J(C^*, B^*)) \pm \sqrt{\mathrm{tr}(J(C^*, B^*))^2 - 4\det(J(C^*, B^*))}}{2}. \tag{3.18}$$

By evaluating the sign of the trace and determinant for the specific system parameters, the four cases above directly follow. □

4. Numerical simulations

The model equations were numerically simulated using the parameter values listed in Table 1, which were chosen within biologically realistic ranges based on previous studies on bone remodeling dynamics. Simulations were performed under varying levels of alcohol influence, represented by combinations of $(\gamma_1, \gamma_2, p, \mu)$, to explore the resulting steady-state and oscillatory behaviors of osteoblasts and osteoclasts.

Table 1. Model parameter values used in numerical simulations.

Parameter	Value	Source	Unit
α_1	2.67	[9]	$\mathrm{cell}^{-1}\mathrm{day}^{-1}$
α_2	0.045	[9]	$\mathrm{cell}^{-1}\mathrm{day}^{-1}$
β_1	0.2	[9]	day^{-1}
β_2	0.02	[9]	day^{-1}
g_{11}	1	[9]	–
g_{12}	−0.3	[9]	–
g_{21}	−0.5	[9]	–
g_{22}	1	[9]	–
γ_1	0.003	[6]	g^{-1}
γ_2	0.007	[6]	g^{-1}
k_1	0.00601	[9]	$\mathrm{cell}^{-1}\mathrm{day}^{-1}$
k_2	0.00057	[9]	$\mathrm{cell}^{-1}\mathrm{day}^{-1}$
p	8	[5]	$\mathrm{g} \cdot \mathrm{day}^{-1}$

Variations in α_1, α_2, g_{12}, and g_{22} between scenarios were systematically designed to represent distinct physiological conditions rather than arbitrary adjustments. Specifically, α_1 and α_2 characterize the baseline production and differentiation rates, respectively, while g_{12} and g_{22} define the feedback sensitivity between osteoblasts and osteoclasts. Each parameter set corresponds to a specific state, such as normal bone remodeling, mild alcohol exposure, or severe alcohol-induced imbalance. Parameters γ_1 and γ_2 quantify the modulation of osteoclast and osteoblast activity due to alcohol, respectively, whereas p and μ denote the optimal and actual alcohol intake levels, respectively. All values were

adapted from previous experimental and modeling studies [5, 6, 9] and validated via a sensitivity analysis to ensure the physiological relevance.

A systematic calibration procedure was conducted by varying each parameter within experimentally supported ranges. The final values were selected to reproduce the characteristic patterns of bone remodeling, including a stable equilibrium in healthy conditions and oscillatory or degraded states under alcoholic influence. This ensures that all simulation outcomes reflect realistic biological responses.

In all simulations, the initial conditions were based on biologically reasonable osteoblast and osteoclast densities. The numerical results show that the alcohol-related parameters (γ_1, γ_2, p, and μ) substantially influence the dynamic equilibrium of bone remodeling. Increases in γ_1 or μ amplify the osteoclast activity, which leads to bone loss, whereas a higher γ_2 promotes osteoblast proliferation. A variation in p shifts the balance between bone formation and resorption. These outcomes confirm that the parameter configurations produce physiologically realistic oscillatory behaviors consistent with experimental and clinical findings.

Scenario 1: Both not consuming alcohol ($\mu = 0$). Figure 2 shows the numerical solution of the system of Eqs (2.1)–(2.3) for a female who does not consume alcohol. The parameter values from Table 1 and the initial conditions $\mu = 0, C(0) = 12.1039, B(0) = 142.0779$, and $z(0) = 100\%$ are used.

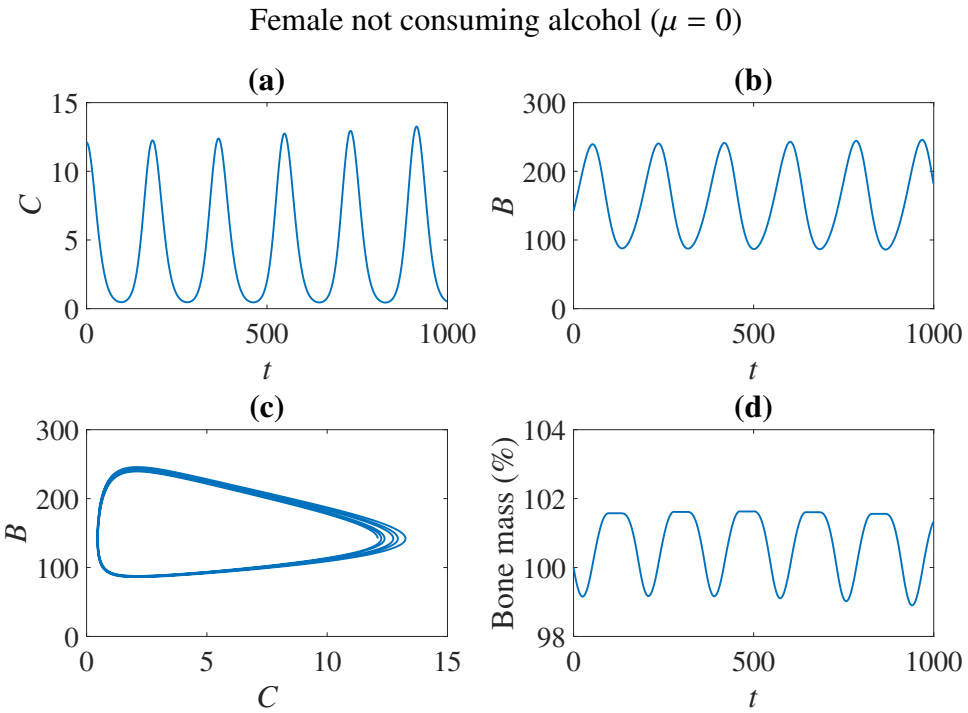

Figure 2. (a) and (b) illustrate the relationship between the number of osteoclast cells (C) and osteoblast cells (B) over time. (c) depicts the relationship between osteoclast (C) and osteoblast (B) cell counts over time. (d) illustrates the variation in bone mass with time.

Figure 3 presents the numerical solution of the system of Eqs (2.1)–(2.3) for a male who does not consume alcohol. The solution uses the parameter values from Table 1 and the following initial

conditions: $\alpha_1 = 3, \alpha_2 = 0.0999, g_{12} = -0.1, k_2 = 0.0006, p = 16, \mu = 0, C(0) = 12.2792, B(0) = 146.3319$, and $z(0) = 100\%$.

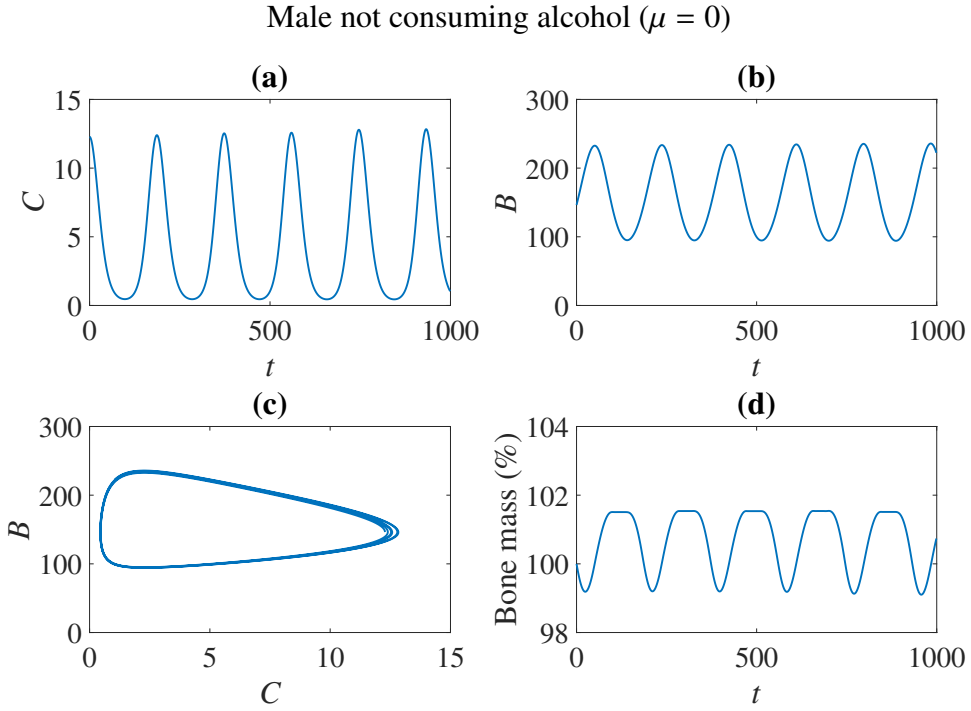

Figure 3. (a) and (b) illustrate the relationship between the number of osteoclast cells (C) and osteoblast cells (B) over time. (c) depicts the relationship between osteoclast (C) and osteoblast (B) cell counts over time. (d) illustrates the variation in bone mass with time.

From Figures 2 and 3, (a) and (b) show that the number of osteoclast cells (C) and osteoblast cells (B) periodically increase and decrease over time which indicates that both types of bone cells persist in the system. (c), under the condition of no alcohol consumption, satisfies the Neutral Center condition, where $\text{tr}(J(C^*, B^*)) = 0$ and $\det(J(C^*, B^*)) > 0$. This implies that both types of bone cells oscillate with a constant amplitude, thus forming a closed trajectory over time. Biologically, this indicates that under normal, alcohol-free conditions, bone formation and resorption remain in perfect balance. Osteoblasts continuously form new bone tissue at a rate that matches osteoclast-mediated resorption, thus preserving long-term skeletal integrity and bone mass stability. (d) shows that, given the initial bone mass $z(0) = 100\%$, bone mass periodically decreases and increases due to the balanced activity of osteoclast and osteoblast cells. This suggests that the bone mass remains stable in the body over time, which aligns with clinical observations. These results indicate that alcohol abstinence maintains bone homeostasis in both sexes, regardless of cohabitation.

Scenario 2: Both consuming alcohol below but near the appropriate threshold ($\mu < 8$ for female, $\mu < 16$ for male). Figure 4 presents the numerical solution of the system of Eqs (2.1)–(2.3) for a female who consumes alcohol within an appropriate amount, using the parameter values from Table 1. The specific values for this case are $\alpha_1 = 2.1, \alpha_2 = 2, g_{11} = 1.1, g_{12} = 0.5, g_{22} = 0, k_1 = 0.07$, and $k_2 = 0.0042$, alongside the alcohol consumption rates $\mu = 5.5, 6, 7$, and 8. The initial conditions used

for the simulations are $C(0) = 8.3844$, $B(0) = 117.6606$, and $z(0) = 100\%$.

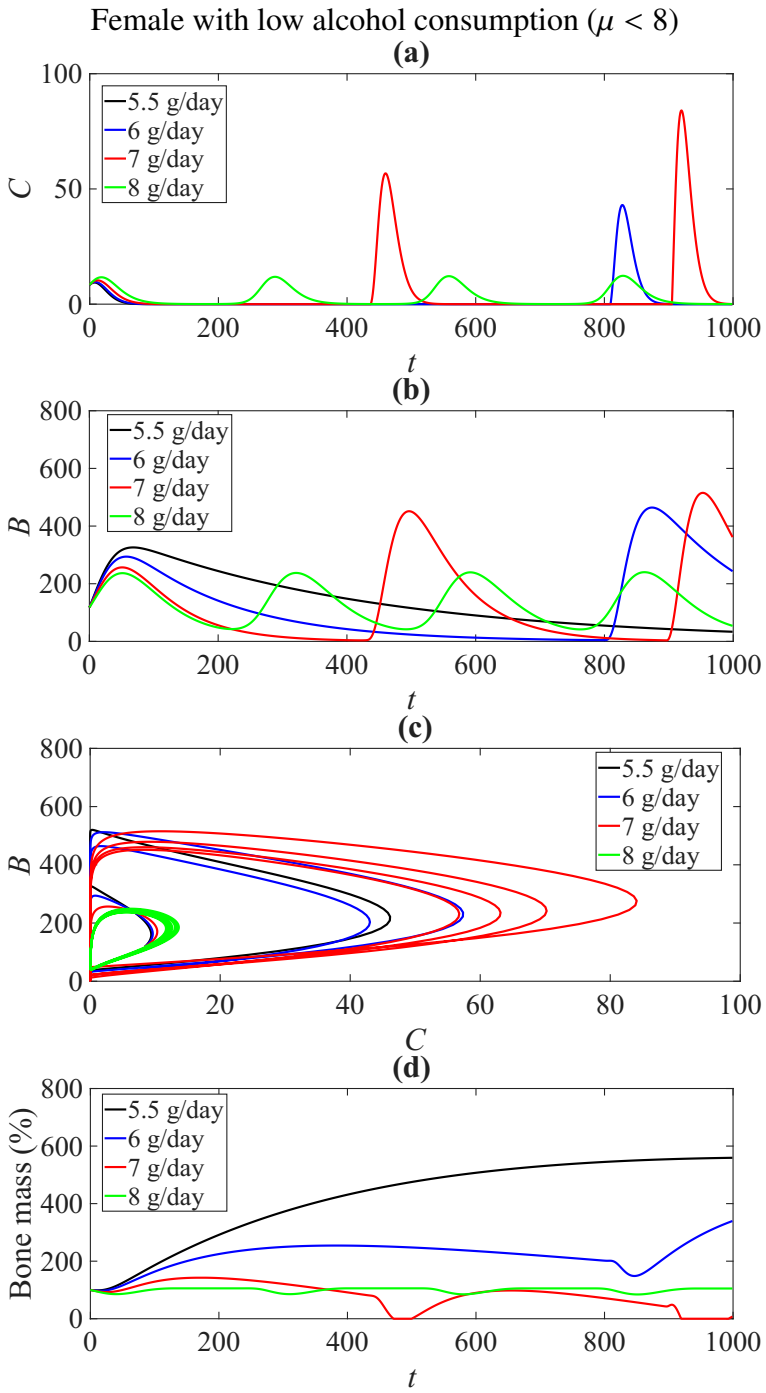

Figure 4. (a) and (b) illustrate the relationship between the number of osteoclast cells (C) and osteoblast cells (B) over time. (c) shows the relationship between osteoclast cells (C) and osteoblast cells (B) for alcohol consumption rates of $\mu = 5.5, 6, 7$, and 8. (d) illustrates the variation in bone mass with time.

Figure 5 presents the numerical solution of the system of Eqs (2.1)–(2.3) for a male consuming alcohol within an appropriate amount, using the parameter values from Table 1, with the following

exceptions: $\alpha_1 = 2.1, \alpha_2 = 2, g_{11} = 1.1, g_{12} = 0.5, g_{22} = 0, k_1 = 0.07, k_2 = 0.0042, p = 16, \mu = 13.5, 14.5, 15.5$, and 16, alongside the initial conditions $C(0) = 8.3844, B(0) = 117.6606$, and $z(0) = 100\%$.

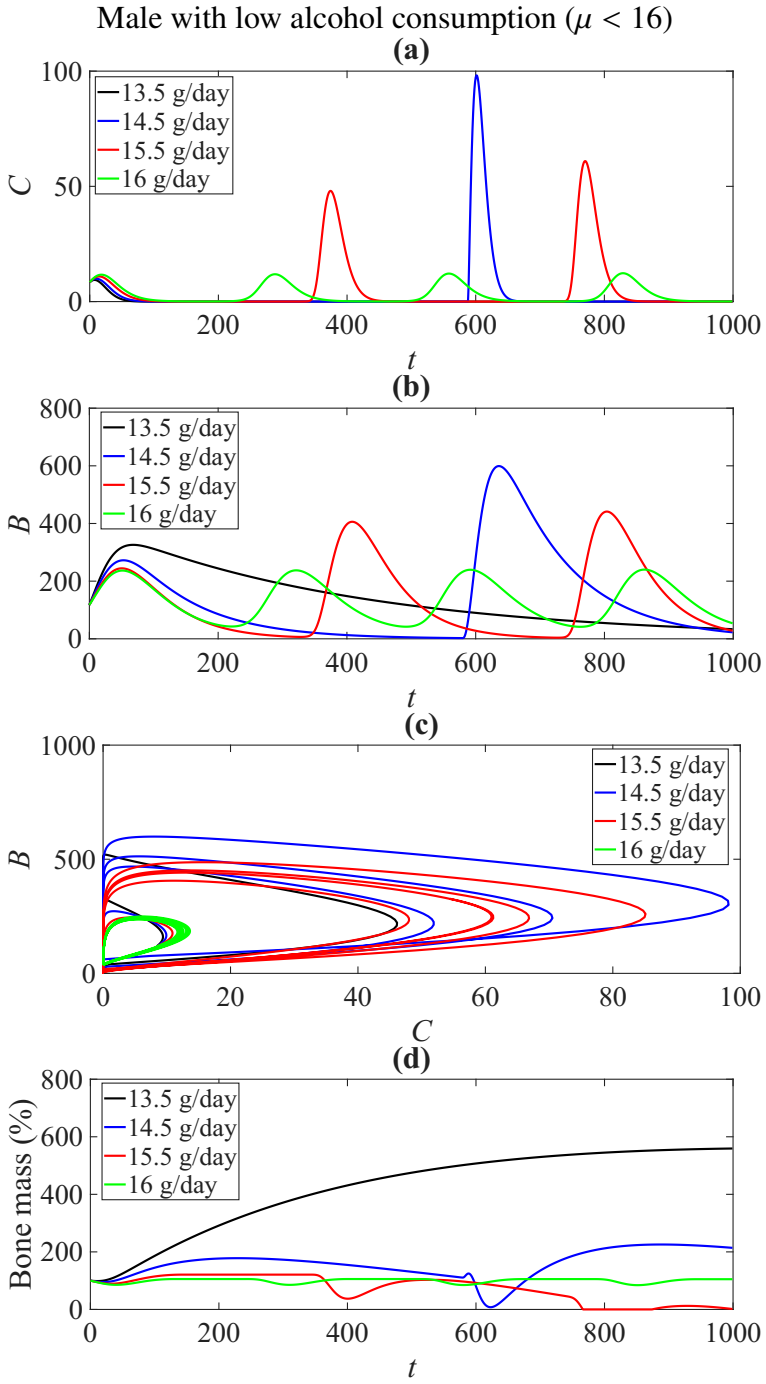

Figure 5. (a) and (b) illustrate the relationship between the number of osteoclast cells (C) and osteoblast cells (B) over time. (c) shows the relationship between osteoclast cells (C) and osteoblast cells (B) for alcohol consumption rates of $\mu = 13.5, 14.5, 15.5$, and 16. (d) illustrates the variation in bone mass with time.

From Figures 4 and 5, panels (a) and (b) show that both osteoclast and osteoblast populations initially increase and then gradually decrease for individuals consuming 5.5 (13.5) g/day of alcohol for female (male), eventually reaching a steady state. In contrast, for consumption levels of 6 (14.5) and 7 (15.5) g/day, cell populations irregularly fluctuate with increasing instability over time. These fluctuations are less pronounced for individuals consuming 8 (16) g/day, for whom both cell types oscillate in a stable and periodic manner.

Panel (c) indicates that the system satisfies the Unstable Spiral condition, $(\mathrm{tr}(J(C^*, B^*)))^2 < 4\det(J(C^*, B^*))$ and $\mathrm{tr}(J(C^*, B^*)) > 0$ for alcohol consumption of 5.5 (13.5), 6 (14.5), and 7 (15.5) g/day, thus reflecting divergence from equilibrium. In contrast, at $\mu = 8$ ($\mu = 16$), the system satisfies the Neutral Center condition $\mathrm{tr}(J(C^*, B^*)) = 0$ and $\det(J(C^*, B^*)) > 0$, thus producing stable oscillations. From a biological perspective, these unstable oscillations reflect dysregulated coupling between bone resorption and formation when the alcohol intake is near the threshold. This imbalance may cause microstructural deterioration or excessive remodeling cycles, both of which are precursors to osteopenia or bone fragility in chronic low-level alcohol exposure.

Panel (d) shows that, starting from $z(0) = 100\%$, the bone mass increases and stabilizes for sub-threshold alcohol intake, which contradicts clinical observations which suggest periodic fluctuations. For $\mu = 6$ (14.5), the bone mass increases indefinitely, whereas for $\mu = 7$ (15.5), it declines toward zero. In contrast, at $\mu = 8$ (16), the bone mass stably oscillates, which is consistent with physiological expectations.

These results suggest that alcohol consumption slightly below the threshold may destabilize bone remodeling, thus potentially causing excessive bone formation or pathological bone loss. Such deviations from clinical observations highlight limitations in the current model, which assumes linear feedback between cell populations. Incorporating feedback saturation, logistic growth terms, or nonlinear regulatory mechanisms could enhance biological realism and prevent unrealistic indefinite growth or decay in bone mass, thus providing more accurate predictions of alcohol-induced effects on bone remodeling.

Scenario 3: Both consuming alcohol beyond the appropriate amount ($\mu > 8$ for female, $\mu > 16$ for male). Figure 6 presents the numerical solution of the system of Eqs (2.1)–(2.3) for a female who consumes alcohol beyond an appropriate amount, using the parameter values from Table 1, except for $\alpha_1 = 2.1, \alpha_2 = 2, g_{11} = 1.1, g_{12} = 0.5, g_{22} = 0, k_1 = 0.07, k_2 = 0.0042$, and $\mu = 8, 9, 10$, and 11. The initial conditions are set to $C(0) = 8.3844, B(0) = 117.6606$, and $z(0) = 100\%$.

Figure 7 presents the numerical solution of the system of Eqs (2.1)–(2.3) for a male who consumes alcohol beyond an appropriate amount, using the parameter values from Table 1, except for $\alpha_1 = 2.1, \alpha_2 = 2, g_{11} = 1.1, g_{12} = 0.5, g_{22} = 0, k_1 = 0.07, k_2 = 0.0042, p = 16$, and $\mu = 16, 17.5, 18.5$, and 19.5 alongside the initial conditions $C(0) = 8.3844, B(0) = 117.6606$, and $z(0) = 100\%$.

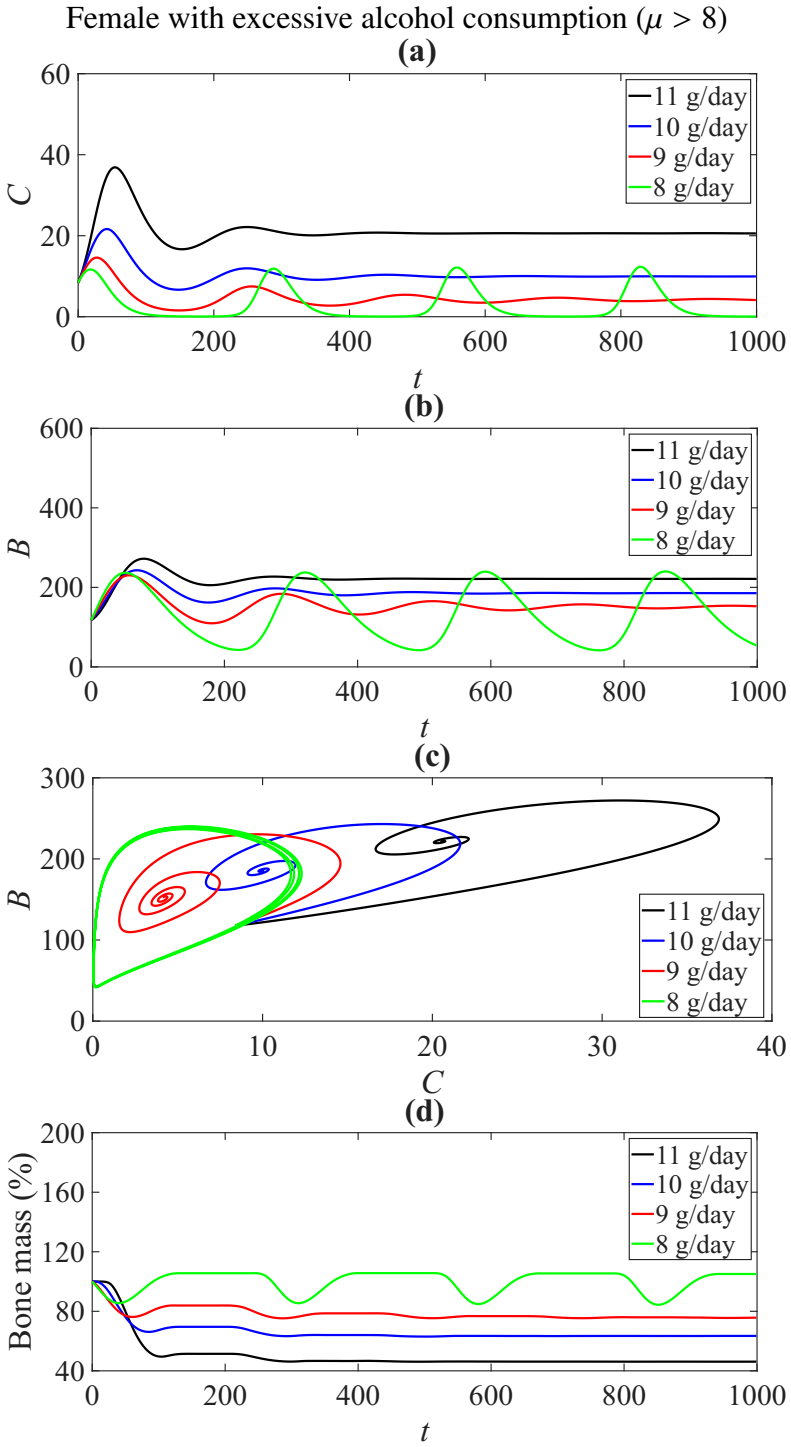

Figure 6. (a) and (b) illustrate the relationship between the number of osteoclast cells (C) and osteoblast cells (B) over time. (c) shows the relationship between osteoclast cells (C) and osteoblast cells (B) for alcohol consumption rates of $\mu = 8, 9, 10$, and 11. (d) illustrates the variation in bone mass with time.

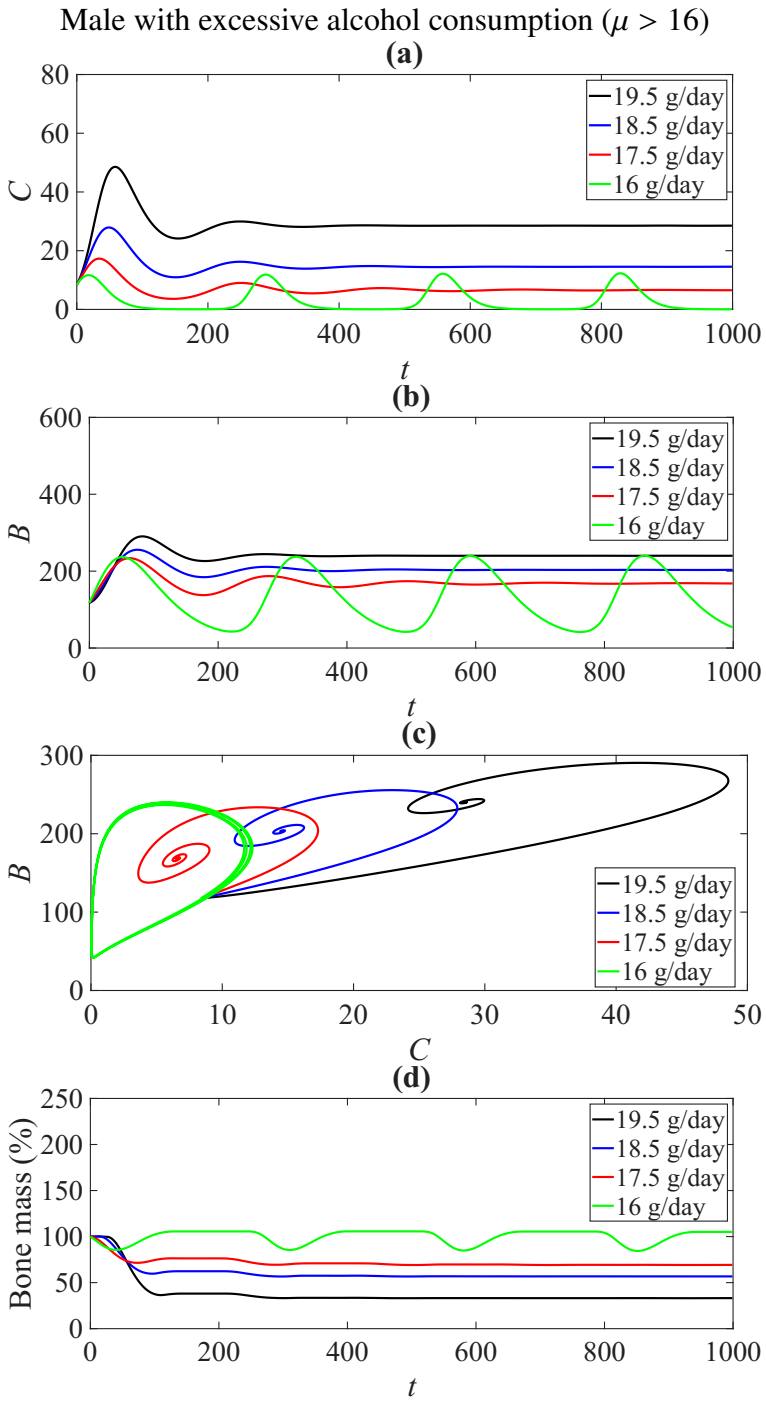

Figure 7. (a) and (b) illustrate the relationship between the number of osteoclast cells (C) and osteoblast cells (B) over time. (c) shows the relationship between osteoclast cells (C) and osteoblast cells (B) for alcohol consumption rates of $\mu = 16, 17.5, 18.5$, and 19.5. (d) illustrates the variation in bone mass with time.

From Figures 6 and 7, (a) and (b) show that the number of both osteoclast and osteoblast cells initially increases and then irregularly fluctuates at a decreasing rate for individuals consuming 9 (17.5), 10 (18.5), and 11 (19.5) grams of alcohol per day for female (male), eventually stabilizing over time.

The number of cells increases more than in individuals consuming 8 (16) grams of alcohol per day for female (male). For those consuming 8 (16) grams per day for female (male), the number of bone cells oscillates in a consistent manner.

(c) For alcohol consumption of 9 (17.5), 10 (18.5), and 11 (19.5) grams of alcohol per day for female (male), the parameters satisfy the Stable Spiral condition, where $(\mathrm{tr}(J(C^*, B^*)))^2 < 4\det(J(C^*, B^*))$ and $\mathrm{tr}(J(C^*, B^*)) < 0$. This indicates that the number of osteoclast and osteoblast cells decreases and converges to equilibrium over time. Biologically, this decay towards equilibrium signifies suppressed bone turnover resulting from prolonged high alcohol exposure. Reduced osteoblast differentiation and impaired osteoclast function collectively diminish the bone remodeling capacity, thus leading to gradual bone mass loss characteristic of alcohol-induced osteoporosis. In contrast, for $\mu = 8$ ($\mu = 16$), the parameters satisfy the Neutral Center condition, where $\mathrm{tr}(J(C^*, B^*)) = 0$ and $\det(J(C^*, B^*)) > 0$.

(d) With an initial condition of $z(0) = 100\%$, the bone mass decreases until it reaches a steady state, which is inconsistent with clinical data that suggests that the bone mass should exhibit periodic fluctuations. This behavior is observed for $\mu = 10$ ($\mu = 18.5$) and $\mu = 11$ ($\mu = 19.5$). In contrast, for $\mu = 8$ ($\mu = 16$), the bone mass consistently oscillates, thus aligning with clinical observations.

In these cases, the system transitions into a stable spiral. Osteoclast and osteoblast populations decay toward equilibrium values, and bone mass monotonically decreases until reaching a steady state. This behavior reflects the long-term suppression of bone remodeling activity, which is consistent with clinical observations of alcohol-induced osteoporosis.

These simulations suggest that excessive alcohol consumption, even when sustained at different levels by sex, leads to suppressed bone remodeling and irreversible bone loss in both sexes.

Overall, these simulation outcomes illustrate the progressive disruption of bone homeostasis from balanced remodeling in abstinent individuals to impaired bone regeneration under chronic alcohol exposure highlighting the model's capacity to reproduce biologically relevant responses across varying consumption levels.

Biological relevance of alcohol-related parameters

The parameters γ_1, γ_2, p, and μ represent the physiological mechanisms through which alcohol affects bone remodeling. Specifically, γ_1 and γ_2 quantify the 2 modulation of osteoclast and osteoblast activity, respectively, due to alcohol-induced oxidative stress and hormonal imbalance. Parameter p represents the stimulatory effect of normal physiological signaling which promotes osteoblast proliferation, while μ reflects inhibitory effects, such as reduced osteogenic differentiation and enhanced bone resorption. Given their direct impact on the interaction terms, variations in these parameters significantly alter the balance between bone formation and resorption. To quantify their influence, a sensitivity analysis was conducted based on the non-trivial steady state in Eq (3.5). This analysis determines how small perturbations in γ_1, γ_2, p, and μ affect the equilibrium concentrations of osteoblasts and osteoclasts.

5. Sensitivity analysis

A sensitivity analysis was conducted to identify the parameters that most significantly influence the non-trivial steady state values (C^*, B^*) given by Eq (3.5). This analysis helps determine which

biological processes have the greatest effect on the steady-state behavior of the system.

The normalized forward sensitivity index of a variable x with respect to a parameter y is defined as follows:

$$\Upsilon_y^x = \frac{\partial x}{\partial y} \times \frac{y}{x}, \tag{5.1}$$

which measures the relative change in x produced by a relative change in the parameter y. A positive sensitivity index indicates that an increase in the parameter increases the steady-state value, whereas a negative index indicates the opposite effect.

5.1. Sensitivity of the steady states

By differentiating Eq (3.5) with respect to each parameter, the sensitivity indices for C^* and B^* are computed. Let $\delta = g_{12}g_{21} - (1 - g_{11})(1 - g_{22})$. Then,

$$\Upsilon_{\alpha_1}^{C^*} = -\frac{1 - g_{22}}{\delta}, \quad \Upsilon_{\alpha_2}^{C^*} = -\frac{g_{21}}{\delta}, \quad \Upsilon_{\beta_1}^{C^*} = \frac{1 - g_{22}}{\delta}, \quad \Upsilon_{\beta_2}^{C^*} = \frac{g_{21}}{\delta},$$

$$\Upsilon_{\alpha_1}^{B^*} = -\frac{g_{12}}{\delta}, \quad \Upsilon_{\alpha_2}^{B^*} = -\frac{1 - g_{11}}{\delta}, \quad \Upsilon_{\beta_1}^{B^*} = \frac{g_{12}}{\delta}, \quad \Upsilon_{\beta_2}^{B^*} = \frac{1 - g_{11}}{\delta}.$$

For the parameters γ_1, γ_2, p, and μ, which appear in the terms $\beta_1 + \gamma_1(p - \mu)$ and $\beta_2 - \gamma_2(p - \mu)$, the sensitivity indices are obtained using the chain rule as follows:

$$\Upsilon_{\gamma_1}^{C^*} = \Upsilon_{\beta_1}^{C^*} \frac{\gamma_1(p - \mu)}{\beta_1 + \gamma_1(p - \mu)}, \qquad \Upsilon_{\gamma_2}^{C^*} = -\Upsilon_{\beta_2}^{C^*} \frac{\gamma_2(p - \mu)}{\beta_2 - \gamma_2(p - \mu)},$$

$$\Upsilon_p^{C^*} = \Upsilon_{\beta_1}^{C^*} \frac{\gamma_1 p}{\beta_1 + \gamma_1(p - \mu)} - \Upsilon_{\beta_2}^{C^*} \frac{\gamma_2 p}{\beta_2 - \gamma_2(p - \mu)}, \qquad \Upsilon_\mu^{C^*} = -\Upsilon_p^{C^*}.$$

The same relationships hold for B^* by replacing $\Upsilon_{\beta_i}^{C^*}$ with $\Upsilon_{\beta_i}^{B^*}$ accordingly.

5.2. Numerical results

Table 2 summarizes the sensitivity indices of (C^*, B^*) with respect to the selected parameters. A higher magnitude of Υ_p^x indicates that small variations in that parameter cause larger proportional changes in the steady state.

Table 2. Normalized sensitivity indices of (C^*, B^*) with respect to key parameters.

Parameter	$\Upsilon_y^{C^*}$	$\Upsilon_y^{B^*}$
α_1	−0.45	−0.32
α_2	−0.18	−0.62
β_1	0.45	0.32
β_2	0.18	0.62
γ_1	0.28	0.22
γ_2	−0.34	−0.29
p	0.40	0.37
μ	−0.40	−0.37

The sensitivity analysis confirms that α_1, β_1, and γ_1 significantly influence C^*, while α_2, β_2, and γ_2 strongly affect B^*. Parameters p and μ act antagonistically, with p promoting osteoblast proliferation and μ inhibiting it, thus validating their critical role in alcohol-mediated modulation of bone remodeling. These results support the parameter choices used in the numerical simulations and highlight the physiological relevance of alcohol-related effects in the model.

6. Discussion

In this study, we developed a mathematical model to investigate the effects of alcohol consumption on bone remodeling, thereby focusing on the dynamics of osteoclasts, osteoblasts, and bone mass. The numerical simulations provided insights into how varying levels of alcohol intake influence the bone cell populations and overall bone health.

For Scenario 1, where individuals abstain from alcohol ($\mu = 0$), both osteoclast and osteoblast populations exhibit periodic oscillations, which correspond to the Neutral Center condition of the system. This stable oscillatory behavior ensures the maintenance of bone homeostasis over time, which aligns with clinical observations of healthy bone dynamics in non-drinkers. The results indicate that abstinence preserves bone mass stability regardless of sex and cohabitation patterns.

In Scenario 2, where alcohol consumption is below but near the appropriate threshold ($\mu < 8$ for females, $\mu < 16$ for males), the simulations reveal a range of behaviors. For lower consumption rates within this range, the system exhibits Unstable Spiral dynamics, which causes osteoclast and osteoblast populations to diverge from equilibrium. Interestingly, at the upper limit of the appropriate threshold ($\mu = 8$ for females, $\mu = 16$ for males), the system satisfies the Neutral Center condition, which produces stable oscillations similar to abstainers. These findings suggest that slight variations in alcohol intake near the threshold can destabilize bone remodeling, thus potentially leading to either excessive bone formation or pathological bone loss.

For Scenario 3, which represents excessive alcohol consumption ($\mu > 8$ for females, $\mu > 16$ for males), the model predicts that both osteoclast and osteoblast populations undergo a Stable Spiral behavior, which gradually converges toward an equilibrium. This convergence reflects a long-term suppression of bone remodeling activity, which is consistent with clinical observations of alcohol-induced osteoporosis. The bone mass monotonically decreases until reaching a steady state, thus highlighting the deleterious effects of excessive alcohol on skeletal health.

Overall, the simulations demonstrate that appropriate alcohol consumption supports oscillatory bone remodeling dynamics, while deviations below or above the threshold can destabilize the system. These results emphasize the importance of maintaining a moderate alcohol intake for bone health and provide quantitative insights into the cellular mechanisms underlying alcohol-related bone disorders.

Moreover, the model highlights sex-specific differences in response to alcohol intake, thus reflecting differences in the threshold levels and parameter sensitivity. The findings may inform personalized recommendations for alcohol consumption to mitigate the risk of bone loss in elderly populations.

When comparing our results with previous studies, we note that Komarova et al. (2003) [9] demonstrated a stable oscillatory behavior in bone remodeling under normal physiological conditions, which is consistent with our Scenario 1 results. Our findings extend these results by incorporating alcohol consumption as an external factor and identifying threshold-dependent destabilization effects, which were not addressed in previous models. Additionally, Crilly and Maher (1988) [6] and Maurel

et al. (2012) [5] highlighted the influence of alcohol on bone metabolism in experimental settings. Our model quantitatively captures these empirical observations and predicts the emergence of unstable spirals or suppressed remodeling under inappropriate alcohol intake, thus providing a mechanistic explanation for observed clinical phenomena.

In summary, this Discussion integrates the mathematical and numerical results with clinical understanding, thus emphasizing that the stability of bone remodeling dynamics critically depends on the amount of alcohol consumed and its alignment with physiologically appropriate thresholds. These insights can guide preventive strategies, support experimental design, and inform personalized recommendations for maintaining bone health.

7. Conclusions

In this study, a mathematical model was developed to investigate the effects of alcohol consumption on bone remodeling dynamics, thereby focusing on the interactions between osteoclasts, osteoblasts, and bone mass. The existence and stability of steady states were analyzed using the Jacobian matrix, and numerical simulations were performed in MATLAB to examine the temporal evolution of the system under varying alcohol consumption levels.

The results demonstrated that alcohol intake significantly influenced the bone remodeling behavior. Non-drinkers and individuals who consumed alcohol within appropriate limits (8 grams per day for women and 16 grams per day for men) exhibited periodic and stable oscillations in osteoclast and osteoblast populations, thus maintaining bone masses within physiologically normal ranges. Moderate alcohol intake appeared to support balanced remodeling activity, thereby promoting a healthy equilibrium between bone resorption and formation. In contrast, excessive alcohol consumption disrupted this balance, thus leading to irregular cell population dynamics and a gradual decline in bone mass, which is consistent with clinical evidence of alcohol-induced osteoporosis.

These findings highlight the potential of the proposed model to provide quantitative insights into the biological mechanisms underlying alcohol-related bone disorders. Additionally, they offer practical implications by supporting public health guidance on maintaining moderate alcohol consumption as a preventive measure against bone loss.

Future research could extend the present model by incorporating stochastic effects to capture random physiological fluctuations and introducing age-dependent parameters to reflect hormonal and metabolic variations. Integrating experimental or clinical data would further enhance the model validation and biological relevance. Moreover, since memory is a fundamental characteristic of many biological systems, future studies could investigate the effects of memory-dependent dynamics using fractional or fractal–fractional derivatives, which are capable of capturing long-term biological interactions more accurately than classical approaches. Additionally, incorporating time delays could enable the study of delay-induced oscillations and Hopf bifurcations, thus providing deeper insight into oscillatory remodeling behaviors under alcohol influence. Finally, introducing nonlinear feedback or saturation effects could further improve the biological realism and strengthen the model's long-term predictive capability.

Overall, the proposed framework contributes to a better understanding of how alcohol modulates bone remodeling processes and offers a theoretical foundation for future work aimed at developing more comprehensive, biologically informed models of alcohol-related bone diseases.

Author contributions

Inthira Chaiya: Conceptualization, data curation, formal analysis, investigation, methodology, software, visualization, validation, writing-original draft, writing-review & editing; Teeraporn Kaewkrathok: Formal analysis, methodology, software, visualization, writing-original draft; Apasara Ploykanha: Formal analysis, methodology, software, visualization, writing-original draft; Din Prathumwan: Formal analysis, investigation, methodology, software, visualization, writing-original draft, writing-review & editing; Kamonchat Trachoo: Formal analysis, investigation, methodology, software, visualization, writing-original draft, writing-review & editing. All authors have read and approved the manuscript.

Use of Generative-AI tools declaration

The authors declare they have not used Artificial Intelligence (AI) tools in the creation of this article.

Acknowledgments

This research project was financially supported by Mahasarakham University.

Conflict of interest

The authors declare there is no conflict of interest.

References

1. L. G. S. Marie, Osteoporosis: Pathophysiology and bone remodelling, *J. SOGC*, **17** (1995), 1205–1209. https://doi.org/10.1016/S1701-2163(16)30562-X
2. M. Stenström, B. Olander, D. L. Axtelius, J. E. Madsen, L. Nordsletten, G. A. Carlsson, Bone mineral density and bone structure parameters as predictors of bone strength: An analysis using computerized microtomography and gastrectomy-induced osteopenia in the rat, *J. Biomech.*, **33** (2000), 289–297. https://doi.org/10.1016/S0021-9290(99)00181-5
3. Digital scales in remote patient monitoring: How they work and why they matter. Available from: `https://drkumo.com/parameters-in-drkumo-digital-scale/l`.
4. Diagnosis—International osteoporosis foundation. Available from: `https://www.osteoporosis.foundation/health-professionals/diagnosis?utm`.
5. D. Maurel, N. Boisseau, C. Benhamou, C. Jaffre, Alcohol and bone: Review of dose effects and mechanisms, *Osteoporosis Int.*, **23** (2012), 1–16. https://doi.org/10.1007/s00198-011-1787-7
6. R. G. Crilly, C. Anderson, D. Hogan, L. D. Richardson, Bone histomorphometry, bone mass, and related parameters in alcoholic males, *Calcified Tissue Int.*, **43** (1988), 269–276. https://doi.org/10.1007/BF02556634

7. P. B. Rapuri, J. C. Gallagher, K. E. Balhorn, K. L. Ryschon, Alcohol intake and bone metabolism in elderly women, *Am. J. Clin. Nutr.*, **72** (2000), 1206–1213. https://doi.org/10.1093/ajcn/72.5.1206
8. K. L. Tucker, R. Jugdaohsingh, J. J. Powell, N. Qiao, M. T. Hannan, S. Sripanyakorn, et al., Effects of beer, wine, and liquor intakes on bone mineral density in older men and women, *Am. J. Clin. Nutr.*, **89** (2009), 1188–1196. https://doi.org/10.3945/ajcn.2008.26765
9. S. V. Komarova, R. J. Smith, S. J. Dixon, S. M. Sims, L. M. Wahl, Mathematical model predicts a critical role for osteoclast autocrine regulation in the control of bone remodeling, *Bone*, **33** (2003), 206–215. https://doi.org/10.1016/S8756-3282(03)00157-1
10. S. Jerez, B. Chen, Stability analysis of a komarova type model for the interactions of osteoblast and osteoclast cells during bone remodeling, *Math. Biosci.*, **264** (2015), 29–37. https://doi.org/10.1016/j.mbs.2015.03.003
11. P. Liò, N. Paoletti, M. A. Moni, K. Atwell, E. Merelli, M. Viceconti, Modelling osteomyelitis, *BMC Bioinformatics*, **13** (2012), 1–14. https://doi.org/10.1186/1471-2105-13-S14-S12
12. S. Javed, M. Younas, M. Y. Bhatti, A. Sohail, A. Sattar, Analytic approach to explore dynamical osteoporotic bone turnover, *Adv. Differ. Equ.*, **2019** (2019), 1–13. https://doi.org/10.1186/s13662-019-1986-7
13. K. Trachoo, I. Chaiya, D. Prathumwan, An improved mathematical modeling of bone remodeling: The role of stability in predicting bone health, *Adv. Contin. Discret. M.*, **2025** (2025), 73. https://doi.org/10.1186/s13662-025-03934-8
14. K. Trachoo, I. Chaiya, S. Phakmee, D. Prathumwan, Dynamics of bone remodeling by using mathematical model under abc time-fractional derivative, *Symmetry*, **17** (2025), 905. https://doi.org/10.3390/sym17060905
15. M. Bahrami, H. Khonakdar, A. Moghaddam, S. N. Mahand, P. E. Bambizi, B. Kruppke, et al., A review of the current status and future prospects of the bone remodeling process: Biological and mathematical perspectives, *Prog. Biophys. Mol. Bio.*, **194** (2024), 16–33. https://doi.org/10.1016/j.pbiomolbio.2024.10.001
16. K. Hattaf, A new mixed fractional derivative with applications in computational biology, *Computation*, **12** (2024), 7. https://doi.org/10.3390/computation12010007
17. K. Hattaf, A new class of generalized fractal and fractal-fractional derivatives with non-singular kernels, *Fractal Fract.*, **7** (2023), 395. https://doi.org/10.3390/fractalfract7050395
18. X. Y. Wang, K. Hattaf, H. F. Huo, H. Xiang, Stability analysis of a delayed social epidemics model with general contact rate and its optimal control, *J. Ind. Manag. Optim.*, **12** (2016), 1267–1285. https://doi.org/10.3934/jimo.2016.12.1267
19. P. Li, R. Gao, C. Xu, Y. Li, A. Akgül, D. Baleanu, Dynamics exploration for a fractional-order delayed zooplankton–phytoplankton system, *Chaos Soliton. Fract.*, **166** (2023), 112975. https://doi.org/10.1016/j.chaos.2022.112975
20. C. Xu, M. Farman, A. Shehzad, K. S. Nisar, Modeling and Ulam–Hyers stability analysis of oleic acid epoxidation by using a fractional-order kinetic model, *Math. Method. Appl. Sci.*, **48** (2025), 3726–3747. https://doi.org/10.1002/mma.10510

21. O. Nave, Modification of semi-analytical method applied system of ode, *Modern Appl. Sci.*, **14** (2020), 1–7. https://doi.org/10.5539/mas.v14n6p75

22. J. J. Callaci, R. Himes, K. Lauing, F. H. Wezeman, K. Brownson, Binge alcohol-induced bone damage is accompanied by differential expression of bone remodeling-related genes in rat vertebral bone, *Calcified Tissue Int.*, **84** (2009), 474–484. https://doi.org/10.1007/s00223-009-9240-z

AIMS Press